Vol. 14: 309–328, 2022
https://doi.org/10.3354/aei00445

AQUACULTURE ENVIRONMENT INTERACTIONS
Aquacult Environ Interact

Published December 15

Combined models of growth, waste production, dispersal and deposition from cage-cultured Atlantic salmon to predict benthic enrichment

B. T. Hargrave[1,*], R. Filgueira[2], J. Grant[3], B. A. Law[4]

[1]561 Balmy Beach Road, Owen Sound, ON N4K 5N4, Canada
[2]Marine Affairs Program, Dalhousie University, 1355 Oxford St., PO Box 15000, Halifax, NS B3H 1R2, Canada
[3]Department of Oceanography, Dalhousie University, Halifax, NS B3H 4J1, Canada
[4]Fisheries and Oceans Canada, Bedford Institute of Oceanography, Dartmouth, NS B2Y 4A2, Canada

ABSTRACT: Models of particulate waste production and deposition can be used in performance-based management approaches as cost-effective tools to assess environmental effects of open-pen finfish aquaculture. XLDEPMOD is an MS Excel® spreadsheet-based depositional model for predicting particulate organic carbon (POC) waste production and sedimentation from net-pen cultured finfish. Calculations are based on temperature-dependent fish growth and mass-balance calculations of feed input, growth, respiration and 3 size classes of feces. Depth-average and near-bottom directional currents are used to determine waste dispersion by fitted Gaussian distribution functions. Near-bottom velocity and substrate-based resuspension thresholds and loss of deposited waste due to decomposition and consumption by wild fish and invertebrates are used to calculate net POC sedimentation. The model was applied to 2 Atlantic salmon farms in southwestern Bay of Fundy, Canada. Sensitivity analysis showed that reduction in waste flux due to resuspension depends on the magnitude of current and wave-driven bottom shear and mass fractions of feces with different settling velocities. Depending on depth, current speed, substrate type and fecal mass fractions, resuspension can remove up to 80 % of deposited waste from under net-pens. Steep gradients with high rates (>5 g POC m^{-2} d^{-1}) of sedimentation predicted under and close to cages and lower rates (<1 g POC m^{-2} d^{-1}) >50 m away are consistent with published DEPOMOD results and sediment trap observations at the farm sites. The model can be used by regulators to determine if acceptable environmental standards for benthic impacts due to waste deposition from salmon aquaculture are being maintained.

KEY WORDS: Finfish · Particulate organic carbon · Mass balance · Sedimentation · Resuspension

1. INTRODUCTION

Fish farming has many potential environmental effects, including release of particulate and dissolved waste into the marine environment (Rector et al. 2022). Deposition of fish feces and uneaten food can lead to local eutrophication and hypoxic sediments. Previous studies have indicated relationships between particulate waste organic matter deposition and sediment hypoxia (Hargrave 2010). On this basis, models for waste production, particle dispersion and sedimentation from finfish open net-pen culture have been developed over the past 2 decades to predict local (farm-scale) and potential far-field effects of particulate waste release.

Cromey & Black (2005) and Stucchi et al. (2005) described sub-models used in progressive steps to calculate waste production and dispersion around

*Corresponding author: hargraveb@rogers.com

Publisher: Inter-Research · www.int-res.com

fish aquaculture farms. Waste output in these studies was determined either by applying an observed economic food conversion coefficient (ratio of food used to biomass produced) or, alternatively, by mass-balance models to estimate feed input sufficient to reach a desired harvest weight over a specified grow-out period (Stigebrandt et al. 2004, Strain & Hargrave 2005, Wang et al. 2012, 2013, Cubillo et al. 2016).

Calculations of dispersion and sedimentation of waste particles in previous deposition models applied to finfish aquaculture farms are based on the ratio of depth and particle sinking velocity multiplied by a horizontal current (Silvert & Cromey 2001). Lagrangian particle tracking models like DEPOMOD (Cromey et al. 2002a,b, Cromey & Black 2005) and MERAMOD (Cromey et al. 2012) use currents at up to 3 depths. The coupled 3D hydrodynamic–ecological model system SINMOD (Broch et al. 2017) is more complex, with detailed bathymetry and spatially varying currents over a defined model area used to calculate velocity fields and depths that affect particulate waste dispersion.

An alternative way to calculate spatial patterns of salmon aquaculture waste distribution was proposed by Stucchi et al. (2005). The mean and standard deviation of measured east–west and north–south depth-averaged velocity components in this statistical approach are described by 2 normal Gaussian frequency distributions. Waste deposition is then calculated from mass fractions of particles with different settling velocities and depth-average currents over a uniform depth from the centre of a net-pen array in a 2D matrix. Detailed depositional patterns produced by changes in bathymetry in DEPOMOD are not reproduced using this approach but the use of a constant depth reduces computational complexity.

Settling velocities selected for released particles determine waste distribution patterns in these depositional models. Two types of particles (feed and medium sized fecal pellets) are released randomly at fixed time steps over a specific time period in DEPOMOD (Cromey et al. 2002a). Alternatively, Stucchi et al. (2005) used 3 fecal size classes with different mass fractions normally distributed around the mean sinking rate for fecal pellets (3.2 ± 1.1 cm s^{-1}, mean ± SD) applied in DEPOMOD. Recent studies have shown that mass fractions of different sizes of fecal pellets with different settling rates produced by salmonids should be considered to describe dispersion distances and deposition of particulate waste around salmon farms (Reid et al. 2009, Bannister et al. 2016). Resuspension also affects net deposition of waste. A resuspension module in the original version of DEPOMOD (Cromey et al. 2002b) was criticized since a large proportion of released particles was transported outside of the model domain (e.g. Chamberlain & Stucchi 2007, Keeley et al. 2013, Chang et al. 2014a). 'NewDEPOMOD' (SAMS 2019) includes a revised sea-bed process model (Black et al. 2016) with resuspension being turned on and staying on once the current velocity of 9.5 cm s^{-1} is exceeded. Sediment-dependent thresholds for resuspension have also been proposed to provide a more realistic measure of losses of deposited waste due to resuspension (Law et al. 2016, Carvajalino-Fernández et al. 2020).

The present study uses mass-balance calculations to predict waste production by Atlantic salmon *Salmo salar* using a temperature-dependent growth model described by Strain & Hargrave (2005) and 4 waste particle types with different mass fractions and settling rates reported in Bannister et al. (2016). The statistical approach for determining dispersion and sedimentation in Stucchi et al. (2005) is applied in a spreadsheet format that allows input values for any variable to be modified to determine the effects on spatial scales of sedimentation. Contours for different levels of waste deposition applied in the 2D depositional matrix are used to show results for 2 Atlantic salmon farms in Bliss Harbour, the Bay of Fundy, southwestern New Brunswick (SWNB) in eastern Canada. Studies at these farms over the past 2 decades provide background information to compare model output with DEPOMOD results (Chang et al. 2014a) and moored sediment trap observations (Hargrave 1994).

The spreadsheet model is generic in that the temperature-dependent growth and mass-balance calculations for waste production can be applied for any cultured finfish species if food conversion efficiency or mass-balance estimates and seasonal temperatures over the grow-out period are known. Daily waste release is used to determine maximum (worst-case) and average values for sedimentation over the grow-out period. Substrate-based current thresholds for each waste type are applied to calculate losses due to resuspension. Net sedimentation is total sedimentation corrected for this removal with additional losses due to decomposition and consumption by wild fish and invertebrates. The ratio of net to total waste sedimentation (fraction of waste removed) is the site assimilation coefficient (AC). Aquaculture industry managers, government regulators and non-governmental agencies can use the combined models to evaluate new or established salmon farms to assess site suitability for managing negative effects of increased waste deposition. Predicted levels of sedimentation can be used along

with other indicators of salmon aquaculture environmental impacts (Rector et al. 2022) in a performance-based management approach to determine if acceptable benthic habitat standards are being maintained. A working copy of the model is available from the corresponding author.

2. METHODOLOGY

2.1. Study sites

Previous studies of salmon farm–environment interactions have been conducted in Bliss Harbour, SWNB at 2 locations, designated Farm A and B in this study (Fig. 1) (Hargrave et al. 1993, Hargrave 1994, Wildish et al. 2003, 2004, Milligan & Law 2005, Wildish & Pohle 2005, Chang et al. 2014a,b, Wu et al. 2014). Farm A is Site D in Chang et al. (2014a).

Mean water column depth below chart datum (Z_m) for the lowest normal tide is 18.4 m at Farm A (Chang et al. 2014a) and 14 m at Farm B (Hargrave et al. 1993). Mean and large tide ranges of 5.5 and 7.8 m, respectively, are typical for salmon farms throughout SWNB (Wildish et al. 2003, Chang et al. 2014b). Current velocities measured at 1 m depth intervals every 10 or 20 min with acoustic Doppler profiler (ADCP) current meters deployed from 8 June–7 August 2009 (CM383) and 21 September–17 November 2009 (CM409) for near-surface (3.5 m), mid- (7.6 and 8.7 m) and near-bottom (4.6 and 4.7 m above the bottom) near Farm A (Fig. 1) are used for DEPOMOD model calculations described in Chang et al. (2014a). As a result of the availability of current meter data for that site, most of the model scenarios described here are for Farm A.

Cylindrical sediment traps (n = 4) (1:4 diameter:height aspect ratio to prevent resuspension of settled material) were suspended at 13.5 m at 6 locations within, adjacent to and up to 50 m away from the cage array at Farm B from 19–24 August 1990 (Fig. 1) (Hargrave 1994). Currents measured at Farm A in 2009 are assumed to apply at Farm B. The proximity of the 2 farms (~400 m) and ADCP measurements at various locations around Farm A up to ~200 m from net-pens in 2007 and 2009 (Chang et al. 2014a, Wu et al. 2014) support the assumption. Model structure also allows effects of changes in current statistics on waste dispersion to be evaluated. Variables for cage array dimensions and stocking density (SD) were adjusted for conditions at Farm B to allow model output to be compared to sediment trap observations. Net-pens at Farm B had a total bottom area of 3600 m^2 and were arranged in a rectangular array approximated in our calculations by assuming 24 circular cages of 8 m diameter with 5 m separation along and across 2 rows. Bottom sediments comprised predominantly mud (<63 µm) with 20–30% clay (<4 µm) and a small sand fraction (1–2%) are similar at both farm sites (Hargrave et al. 1993, Wu et al. 2014).

2.2. Model structure

Variables and their values (Table 1) were used in Microsoft (MS) Excel® formulae to calculate fish growth from predicted daily water temperature over the grow-out period and mass-balance coefficients for respiration, fecal production and loss of waste feed. Excel formulae used for all calculations are presented in Supplement 1 at www.int-res.com/articles/suppl/q014p309_supp.pdf. Feed intake to meet mass-balance requirements and daily total particulate organic carbon (POC) waste release are expressed as g POC $fish^{-1}$ d^{-1}. Deposition is calcu-

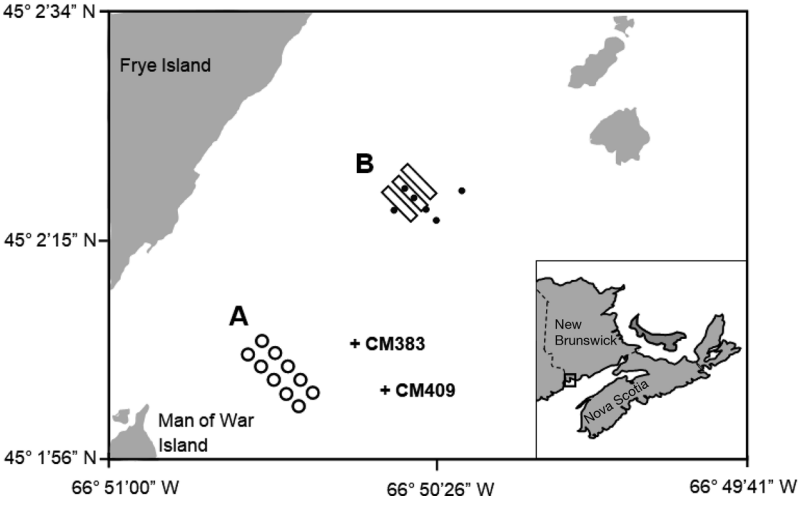

Fig. 1. Locations of 2 Atlantic salmon farms in Bliss Harbour, Passamaquoddy Bay, Bay of Fundy (rectangle in the inset map). Previous studies at Farm A (circles) are described in Chang et al. (2014a) and Wu et al. (2014) and at Farm B (rectangles) in Hargrave et al. (1993) and Hargrave (1994). (+) indicates positions of acoustic Doppler current profiler moorings at sites CM383 (8 June–7 August 2009) and CM409 (21 September–17 November 2009) described in Chang et al. (2014a). Filled circles: locations of sediment trap moorings at Farm B under, adjacent to and +25 and +50 m from the net-pen array described in Hargrave (1994)

Table 1. Variables used to calculate salmon growth, particulate waste production, dispersion and total and net sedimentation for 2 Atlantic salmon farms (A and B) in Bliss Harbour, Bay of Fundy (Fig. 1). POC: particulate organic carbon. Data sources: (1) Chang et al. (2014a); (2) parameters for current statistics for time periods A (CM383) (June–August 2009) and B (CM409) (September–November 2009) described in Table 2; (3) Robinson (2022) and Fig. 3; (4) Wu et al. (2014); (5) Strain & Hargrave (2005); (6) Wang et al. (2012, 2013); (7) Bannister et al. (2016); (8) Carvajalino-Fernández et al. (2020); (9) Cromey et al. (2002a); (10) Stucchi et al. (2005); (11) Hargrave (1994); (12) Callier et al. (2018); (13) Riera et al. (2017); (14) Sutherland et al. (2006); (15) Law et al. (2014, 2016); (16) Adams et al. (2020). Numbers in parentheses represent alternative values for time periods A and B (Table 2). a: assumed or calculated values

Symbol	Description	Value	Source
Site physical characteristics			
Z_m	Mean lowest normal tide depth below chart datum within the farm lease (m)	18.4	1
μ_{EW}	Mean depth-average east–west current velocity (cm s^{-1})	0.346 (1.31)	2
σ_{EW}	Standard deviation of east–west current velocity (cm s^{-1})	4.05 (5.20)	2
μ_{NS}	Mean depth-average north–south current velocity (cm s^{-1})	–0.399 (1.05)	2
σ_{NS}	Standard deviation of north–south current velocity (cm s^{-1})	5.03 (4.27)	2
$f_{\bar{U}>35}$	Fraction of time near-bottom currents >35 cm s^{-1}	0 (0)	2
$f_{\bar{U}>22.5}$	Fraction of time near-bottom currents >22.5 cm s^{-1}	0 (0.015)	2
$f_{\bar{U}>15}$	Fraction of time near-bottom currents >15 cm s^{-1}	0.03 (0.176)	2
$f_{\bar{U}>9.5}$	Fraction of time near-bottom currents >9.5 cm s^{-1}	0.113 (0.499)	2
$f_{\bar{U}>5}$	Fraction of time near-bottom currents >5 cm s^{-1}	0.585 (0.836)	2
T_{max}	Maximum annual water temperature (°C)	12.83	3
T_{min}	Minimum annual water temperature (°C)	0.75	3
JD_{Tmin}	Julian Day for minimum temperature	70	3
B_{sub}	Bottom substrate type (>50%) (1: mud; 2: sand; 3: gravel)	1	4
Farm variables			
APL	Allowable production limit (smolt stocking number)	3.0×10^4 (3.3×10^3)	1, a
f_{mort}	Fraction of biomass lost to mortality during the grow-out period	0.15	1
D	Distance in NS and EW directions from centre of net-pen array (m)	100–500	a
NP_n	Net-pen number stocked	10	1
NP_d	Net-pen diameter (m)	22.3	1
NP_z	Net-pen side-wall depth (m)	10	1
NP_{nl}	Number of net-pens along one row of the array length	5	1
NP_{nw}	Number of net-pens across the array width	2	1
NP_{dl}	Distance between adjacent net-pens along rows (m)	25	1
NP_{da}	Distance between adjacent net-pens across rows (m)	150	1
NP_a	Angle (0–180°) of the longitudinal axis of the cage array relative to north (0: perpendicular; 90: parallel)	–45	1
Fish growth and waste production			
JD_S	Julian Day stocking initiated	120	1
W_i	Initial smolt wet weight (g $fish^{-1}$)	90	5
GP	Grow-out period (days)	791	1
TGC	Thermal-unit growth coefficient to achieve W_f ($g^{1/3}$ $°C^{-1}$ d^{-1})	0.002368	a
W_f	Final (harvest) wet weight (kg $fish^{-1}$)	4.96	1, 5
DM_{feed}	Fraction of dry matter in feed	0.90	5, 6
DM_{fish}	Fraction of dry matter in fish	0.36	5, 6
f_{Cfish}	Fraction of POC fish (dry weight)	0.54	5, 6
f_{Cfeed}	Fraction of POC in feed (dry weight)	0.51	5, 6
f_{Cinput}	Fraction of POC in feed input retained as growth	0.38	5, 6
$f_{Crespired}$	Fraction of POC in feed input respired	0.40	5, 6
f_{Cfeces}	Fraction of POC in feed input released as feces	0.19	5, 6
$f_{Cwastefeed}$	Fraction of POC in feed input as waste feed	0.03 (0.15)	1 (5, a)
Particulate waste total sedimentation			
f_{feces1}	Fraction of total feces as large pellets (waste type 2)	0.66 (0)	7, 8 (9, 10)
f_{feces2}	Fraction of total feces as small pellets (waste type 3)	0.25 (1.0)	7, 8 (9, 10)
f_{feces3}	Fraction of total feces as fragment fecal material (waste type 4)	0.09 (0)	7, 8 (9, 10)
w_{pt1}	Settling velocity of waste feed (waste type 1) (cm s^{-1})	11 (10)	7–10
w_{pt2}	Settling velocity of large fecal pellets (waste type 2) (cm s^{-1})	7.5 (3.2)	7, 8 (9, 10)
w_{pt3}	Settling velocity of small fecal pellets (waste type 3 (cm s^{-1})	3.0 (3.2)	7, 8 (9, 10)
w_{pt4}	Settling velocity of fragmented fecal material (waste type 4) (cm s^{-1})	0.5 (3.2)	7, 8 (9, 10)
CS_{ref}	Background sedimentation (reference area in Bliss Harbour) (g POC m^{-2} d^{-1})	0.30	11
Particulate waste net sedimentation			
f_{decomp}	Fraction of POC in waste decomposed (loss d^{-1})	0.1	5
f_{cons}	Fraction of POC in waste feed consumed by native marine fauna (loss d^{-1})	0.5	a
vr_{mwp1}	Erosion velocity for initiating w_{pt1} resuspension on mud (substrate type 1) (cm s^{-1})	15	8, 14–16
vr_{swp1}	Erosion velocity for initiating w_{pt1} resuspension on sand (substrate type 2) (cm s^{-1})	22.5	8, 14–16
vr_{gwp1}	Erosion velocity for initiating w_{pt1} resuspension on gravel (substrate type 3) (cm s^{-1})	35	8, 14–16
vr_{mwp2}	Erosion velocity for initiating w_{pt2} resuspension on mud (substrate type 1) (cm s^{-1})	15	8, 14–16
vr_{swp2}	Erosion velocity for initiating w_{pt2} resuspension on sand (substrate type 2) (cm s^{-1})	22.5	8, 14–16
vr_{gwp2}	Erosion velocity for initiating w_{pt2} resuspension on gravel (substrate type 3) (cm s^{-1})	35	8, 14–16
vr_{wp3}	Erosion velocity for initiating w_{pt3} resuspension (all substrate types) (cm s^{-1})	9.5	8, 14–16
vr_{wp4}	Erosion velocity for initiating w_{pt4} resuspension (all substrate types) (cm s^{-1})	5.0	8, 14–16

lated from depth, mean and standard deviations of east–west (u) and north–south (v) current velocities described by normal Gaussian distributions and waste particle settling speeds (Stucchi et al. 2005). Total waste production is corrected for losses due to resuspension, decomposition and consumption by wild fish and invertebrates to calculate net waste sedimentation. Contour plots with conditional formatting for different levels of deposition around net-pens in a multi-cage array are created using 2D x–y matrices for total and net deposition for all waste particle types. Probability values for deposition of each waste type within a cell multiplied by total waste production for each particle type are summed to calculate total waste sedimentation in the area of each cell within the matrix. An example of a summary worksheet for major model outputs is shown in Supplement 2 at www.int-res.com/articles/suppl/q014p309_supp.pdf.

2.3. Statistical and sensitivity analysis

SYSTAT® 2010 (SYSTAT Software) was used to derive Gaussian distribution parameters fitted to observed current velocity distributions. Regression analysis was performed within the Excel chart function for x–y scatterplots. Sensitivity of model output to changes in individual variables was assessed by adding and subtracting maximum and minimum values representing ranges of uncertainty (ΔX) around mean values for variables in Table 1. Results are expressed as percent change in contour areas for sedimentation rates >5 g POC m^{-2} d^{-1} relative to the area for this level of deposition when the mean value for each variable was used for calculations. Sedimentation rate thresholds from <0.3 to >10 g POC m^{-2} d^{-1} are known to induce hypoxic/anoxic conditions in surface marine sediments associated with changes in geochemical variables and macrofauna community composition in SWNB (Wildish et al. 2003, Holmer et al. 2005, Wildish & Pohle 2005, Hargrave 2010, Chang et al. 2014a).

3. RESULTS AND DISCUSSION

3.1. Fish growth and waste production

A cosine function (Eq. S1 in Supplement 1) is used to predict seasonal changes in surface water temperature using annual maximum (12.83°C) and minimum (0.75°C) values. Predicted temperatures were closely correlated (r^2 = 0.977) with observed surface temperature reported for 2014–2015 in Robinson (2022) (Fig. 2A). No water temperature data is available for the summer and fall periods in 2009 when ADCP current data used for calculations in our study was obtained.

Predicted values for monthly average daily feeding rates (Fig. 2B) are based on the licensed stocking level (allowable production limit, APL) (Farm A: 300 000 fish; Farm B: 132 000 fish) increased by 10% to account for initial smolt mortality (Table 1). The average values for mass-balance coefficients from Norwegian salmon farms (Wang et al. 2012) that we applied follow seasonal temperatures as would be expected based on growth rates determined by changes in daily temperature (Fig. 2C). Actual feed input by the site operator (January 2006–July 2007), summarized from Chang et al. (2014a) and B. Chang (pers. comm.), reached maxima between September and November 2006 and at the end of the grow-out period in June 2007. This was the month before harvesting began (Fig. 2B) and the maxima coincide with peaks in growth rate (Fig. 2C). When waste feed, assumed to be 3% of feed input, was added to the industry-provided estimate of feed supply, predicted and observed values were positively correlated (r^2 = 0.828). Periods of maximum feed input (~7000 kg $farm^{-1}$ d^{-1}), considered to be the worst-case scenario for maximum waste production, occurred at times of peak fish growth and waste production (Fig. 2C,D).

Strain & Hargrave (2005) fitted a thermal-unit growth coefficient (TGC) of 2.65 × 10^{-3} g⅓ $°C^{-1}$ d^{-1} to data in Peterson et al. (2001) to model salmon growth at a typical farm in SWNB. The adjusted coefficient in our study (2.37 × 10^{-3} g⅓ $°C^{-1}$ d^{-1}) (Table 1) is slightly lower, but there are differences in the maximum–minimum temperature range, smolt stocking weight and harvest weight used in our calculations. Seasonal changes in biomass with peaks in growth in the first and second year of production in August–September, the period of maximum temperature, closely approximate (±5%) values predicted for the first few months after stocking reported in Peterson et al. (2001) (Fig. 2C). The growth trajectory is similar to observations at other farms in SWNB where salmon are known to attain a wet weight of approximately 5 kg after 21–24 mo (Strain & Hargrave 2005). The lag between maximum water temperatures in August–September (Fig. 2A) and maximum waste production in September–October (Fig. 2D) reflects the fact that biomass in fish is increasing fast enough at this time of the year to more than compensate for small decreases in water temperature.

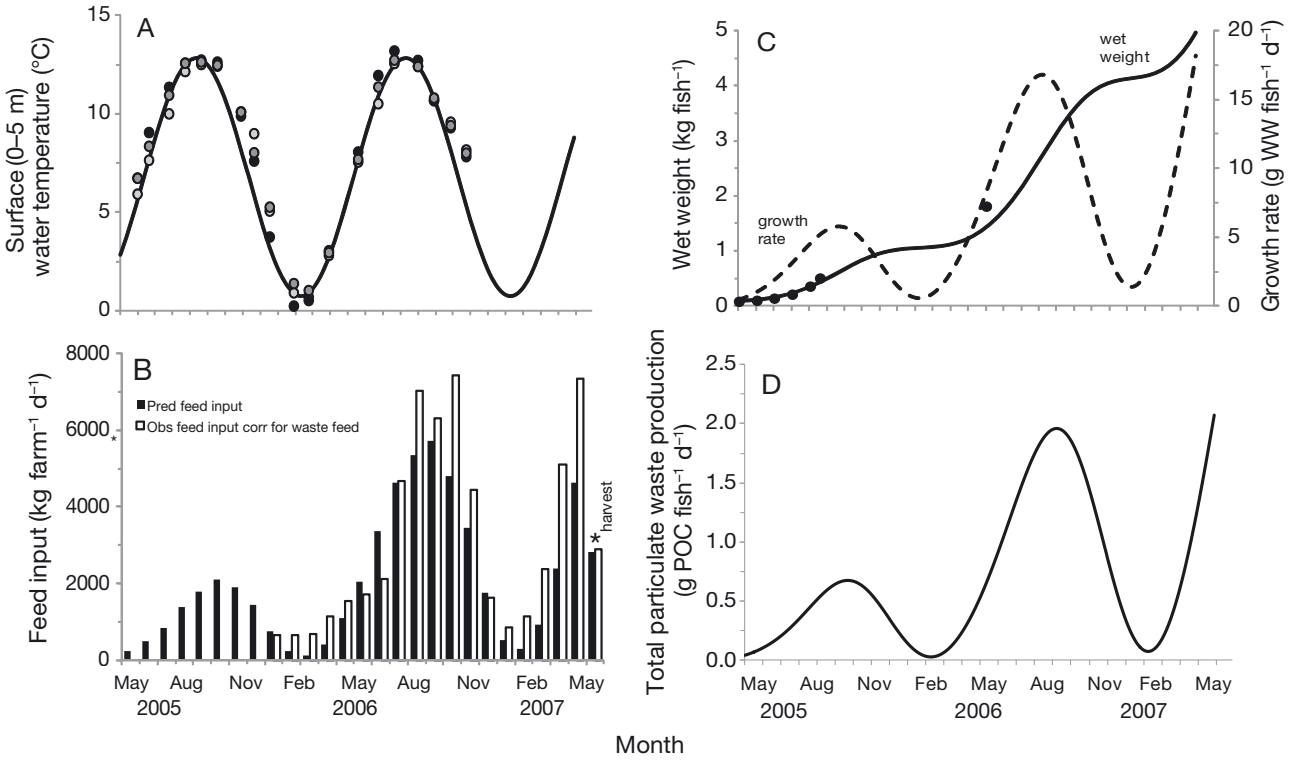

Fig. 2. (A) Variations in surface (0–5 m) temperature in Passamquoddy Bay near Bliss Harbour calculated using a cosine function (Eq. S1 in Supplement 1) (solid line) with annual maximum (12.83°C) and minimum (0.75°C) temperatures. Data from 3 monitoring stations (filled circles) in Passamaquoddy Bay close to Bliss Harbour in 2014 and 2015 (Robinson 2022). (B) Filled bars: predicted feed input required for growth calculated from mass balance coefficients; unfilled: industry reported monthly daily average feed rates from Chang et al. (2014a). (C) Wet weight and daily growth rate calculated using thermal growth and mass-balance coefficients to yield a harvest wet weight of 4.96 kg over 791 d. Filled circles: predicted weight from Peterson et al. (2001) using a Q_{10} growth model. (D) Total particulate waste (feces and waste feed) production during the grow-out period based on mass-balance coefficients. Variable input values for Farm A in Table 1

Other temperature-sensitive growth models have been used to predict growth of cage-cultured finfish (Brigolin et al. 2010, Føre et al. 2016). Aunsmo et al. (2014) found that the TGC model was sensitive to harvest weight and mean water temperature but was moderately successful and similar to 2 other methods for predicting Atlantic salmon growth in Norwegian fish farms. Growth rates modelled in our study varied between 0.4 and 1.4% wet weight d^{-1} during the first year with a maximum of 0.7% d^{-1} in the second year of production (Fig. 2C). The range of values (~0.2–1.5% d^{-1}) and seasonal cycle derived from the TGC model are comparable to those from a temperature-corrected Q_{10} allometric model for salmon production in SWNB (Strain & Hargrave 2005). The TGC model does not require prior knowledge of the economic feed conversion coefficient (wet weight of feed to fresh weight produced ratio) (FCR) often used to estimate feed input (Strain & Hargrave 2005). The FCR calculated for Farm A using our model (1.09) is similar to 1.06 and 1.10 cited as industry averages for SWNB by Stewart (2005) and Strain & Hargrave (2005), respectively.

3.2. Statistical dispersion model

Frequency distributions for current velocity in u and v directions (Fig. 3A,C) were well represented by normal Gaussian distributions (r^2 = 0.995 and 0.997, respectively) (Fig. 3B,D). The depth-averaged mean velocities ($\bar{U}_{mean}$, cm s^{-1}) and standard deviations between 8 June and 7 August 2009 were significantly lower than between 21 September and 18 November 2009 (Fig. 3, Table 2). The difference in current statistics creates 2 scenarios for waste dispersion illustrated in the DEPOMOD output in Chang et al. (2014a). Accelerated current velocities under net-pens and reduced currents due to side-wall drag effects in surface layers were observed when cage length is greater than half the water depth at Farm A (Wu et al. 2014). To account for these pen-related

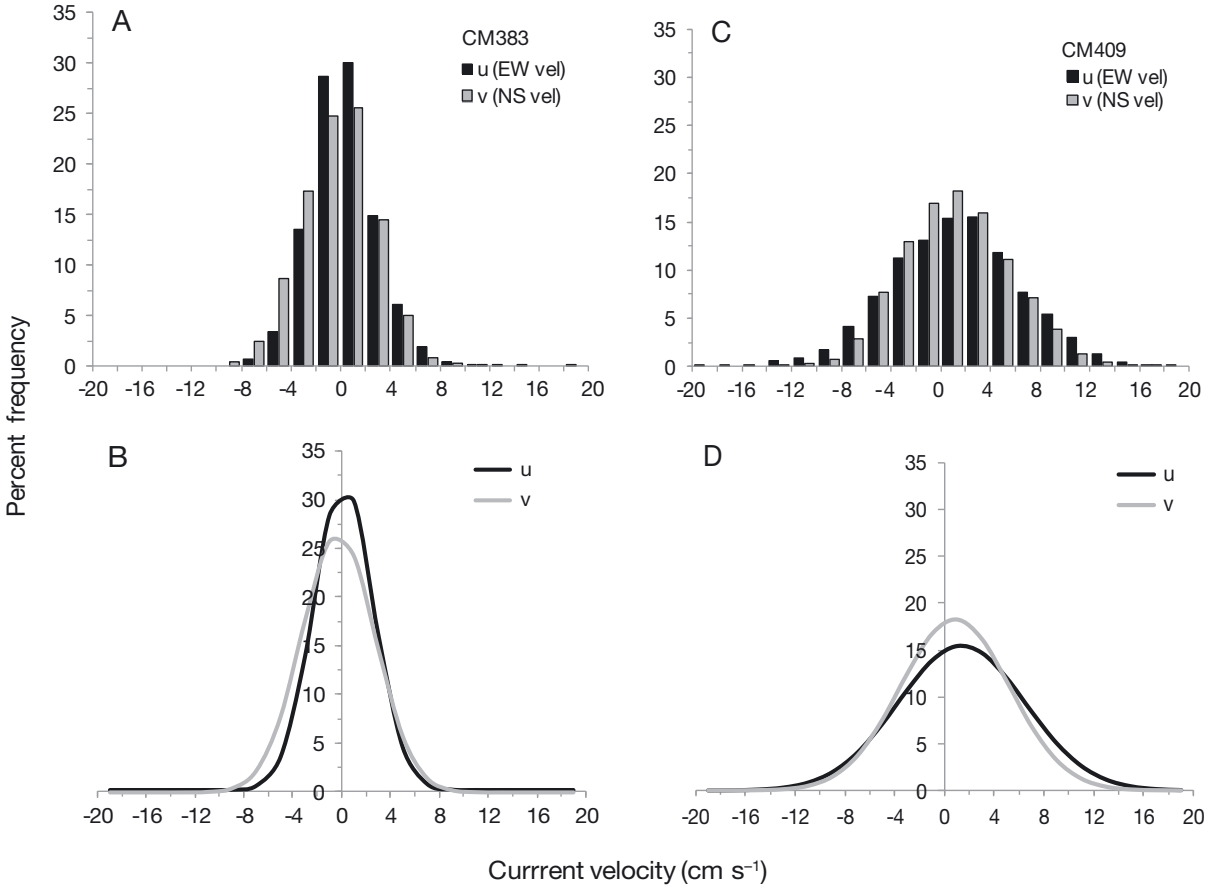

Fig. 3. Data from upward facing acoustic Doppler current profiler (ADCP) CM383 and CM409 moorings in Bliss Harbour in 2009 (Fig. 1, Table 2) summarized from Chang et al. (2014a). (A,B) Frequency distribution for average (near-surface, mid- and near-bottom depths) directional velocity components for ADCP mooring CM383 and fitted normal Gaussian distribution functions for east–west (*u*): $y = 1.18 + 31.47 \times \exp\{-0.5 \times [(x + 0.15) / 2.45]^2\}$ ($r^2 = 0.997$) and north–south (*v*): $y = -0.03 + 26.56 \times \exp\{-0.5 \times [(x - 0.28) / 3.02)^2]\}$ ($r^2 = 0.997$) velocities. (C,D) Frequency distribution for depth-average velocity components for ADCP mooring CM409 and normal Gaussian distribution functions for *u*: $y = 0.06 + 15.43 \times \exp\{-0.5 \times [(x + 1.36) / 5.11)^2]\}$ ($r^2 = 0.995$) and *v*: $y = -0.04 + 18.33 \times \exp\{-0.5 \times [(x + 0.83) / 4.39]^2\}$ ($r^2 = 0.997$) velocities

changes, current velocities from the surface to 10 m (side-wall depth) were reduced by half and currents +4.6 and +7.6 m above bottom were increased by a factor of 2. The modified current statistics with percent of time currents exceed substrate-based thresholds for resuspension show the contrasting flow conditions for the 2 current meter mooring periods (Table 2).

The percent of time that near-bottom (+4.7 m) currents exceed substrate-based resuspension thresholds with higher currents in September–November is greater than during the period of lower currents in June–August (Table 2). The increase is greater when near-bottom velocities are doubled due to cage effects. For example, the 9.5 cm s^{-1} threshold, used by Chang et al. (2014a) for resuspension as the default value in DEPOMOD, increases in the June–August period from 11.3% to61.8% due to accelerated near-bottom currents. An even greater increase (49.9 to 85.3%) occurs with the higher currents during the September–November period.

3.3. Sensitivity of model output to changes in input variables

Maximum changes in the >5 g POC m^{-2} d^{-1} depositional area for total waste sedimentation occur when mean depth (Z_m) and $\bar{U}_{mean}$ are increased and decreased by the values for uncertainty indicated in Table 3. The sensitivity of model output to these 2 variables is expected since horizontal displacement for deposited particles depends on the vertical fall distance, particle settling velocity and standard deviations for currents (Eqs. S3 & S4 in Supplement 1). Changes in SD that determine total biomass on a

Table 2. Depth (Z; –: below surface; +: above bottom), mean and median current speed ($\bar{U}$), mean (μ) and standard deviation (σ) for east–west (EW) and north–south (NS) velocity components and the percent of time near-bottom $\bar{U}_{mean}$ (cm s^{-1}) exceeded thresholds obtained from 2 bottom-moored acoustic Doppler current profilers (ADCP) (CM383 and CM409) for 2 time periods at Farm A (Fig. 1) in Bliss Harbour in 2009 (data summarized from Chang et al. 2014a). Depth averages are for near-surface, mid- and near-bottom depths. (*) indicates u and v near-surface velocities decreased (×0.5) and mid- and near-bottom velocities increased (×2) to account for side-wall drag effects within and under the net-pen array (Wu et al. 2014). Frequency distributions for μ and σ velocity values are shown in Fig. 3

Z (m)	$\bar{U}_{mean}$ (cm s^{-1})	$\bar{U}_{median}$ (cm s^{-1})	μ_{EW} (cm s^{-1})	μ_{NS} (cm s^{-1})	σ_{EW}	σ_{NS}	Percent of time $\bar{U}_{mean}$ >5	>9.5	>15	>22.5	>35
(A) (CM383) 8 June–7 August 2009											
–3.5	5.30	4.43	–0.160	–1.661	5.02	3.90					
+7.6	4.98	4.52	0.234	–0.584	3.75	4.28					
+4.7	5.89	5.70	0.765	0.950	3.77	4.29	58.5	11.3	0.3	0	0
Depth-average	5.38	5.15	0.346	–0.399	4.05	5.03					
–3.5*	2.65	2.22	–0.008	–0.830	2.51	1.95					
+7.6*	9.95	9.04	0.467	–1.168	7.51	8.56					
+4.7*	11.78	5.70	1.530	1.900	7.54	8.58	87.4	61.8	27.9	4.4	0.1
Depth-average*	8.21	7.87	0.700	0.007	8.10	10.06					
(B) (CM409) 21 September–17 November 2009											
–3.5	8.62	7.79	1.032	0.080	7.54	6.66					
+7.6	8.80	8.10	1.318	1.293	7.32	6.76					
+4.7	10.10	9.49	1.471	0.949	8.28	7.54	83.6	49.4	17.6	1.5	0
Depth-average	9.20	8.89	1.310	1.051	5.20	4.27					
–3.5*	4.31	3.89	0.516	0.402	3.77	3.33					
+7.6*	17.61	16.20	2.636	2.586	14.64	13.52					
+4.7*	20.20	18.98	2.943	1.898	16.53	15.07	96.3	85.3	65.0	37.6	9.6
Depth-average*	14.19	13.68	2.108	1.703	8.00	6.66					

farm and seasonal maximum (T_{max}) and minimum (T_{min}) water temperature that affect growth and waste production result in smaller changes in the contour area. The fractions of feed input used for growth (f_{Cinput}) and released as feces (f_{Cfeces}) are the 2 mass-balance coefficients with the greatest effect on waste production. Changes in the amount of feed input released as unconsumed feed pellets ($f_{Cwastefeed}$) have minimal effect on model output since the rate is small relative to the amounts of feed used for growth, respiration and fecal production.

Contour areas for >5 g POC m^{-2} d^{-1} are primarily determined by the relatively large mass fraction (0.66) assigned to rapidly settling fecal pellets (w = 7.5 cm s^{-1}) deposited with minimum horizontal displacement. The relatively shallow water in Bliss Harbour results in the fecal pellets sedimenting immediately under or adjacent to the net-pen array with minimal lateral transport. Increasing the faster settling fraction and decreasing the proportion of slower settling feces decreases the footprint area (–17%) (Table 3) since more of the waste released is concentrated in the more rapidly settling feces. Uncertainty in lower mass fractions and settling rates of smaller fecal pellets and disaggregated fecal matter have similar but smaller effects on the contour area since the waste footprint is determined by the total flux of combined fecal size categories.

Uncertainty in variables associated with losses from total waste flux affecting net sedimentation results in changes in the >5 g POC m^{-2} d^{-1} footprint of a similar magnitude to changes in other variables (Table 3). Variation due to decreasing and increasing the percent daily losses due to decomposition result in an approximately proportional change (+9.5 to –14.3%) since loss is scaled to the amount removed. Changing the proportion of waste feed consumed by natural populations affects the amount of waste feed deposited, but the contour area for flux >5 g POC m^{-2} d^{-1} does not change as the amount of waste input from this source is small relative to total fecal waste production. Altering substrate-related resuspension thresholds changes contour areas as expected by increasing or decreasing the amount of deposited waste removed. When resuspension thresholds for all substrates are lowered, the maximum flux contour area is decreased (–19%). When resuspension thresholds are increased, especially for sand and gravel, the contour areas increase (29 and 48%) as a result of less resuspension and dispersion.

Table 3. Sensitivity of model output to changes in input variables for Farm A shown in Table 1. Percent change in contour areas is relative to baseline values for maximum total waste flux >5 g particulate organic carbon (POC) m^{-2} d^{-1} (1.08 ha) for a mean depth-average current ($\bar{U}_{mean}$) of 9.20 cm s^{-1} (CM409; Table 2) and mass fractions for 3 fecal waste types (Table 1). Selection of 300 m for the distance from the center of the array to the model boundary (*D*) (see Supplement 1) resulted in all waste being deposited within the model area. Net-pen number, dimensions and spacing characteristics were unchanged when values for each variable were altered by (ΔX). Stocking density (SD) (300 000) was altered by changing the allowable production limit ±14%. Brackets indicate groups of variables where the sum of fractions was maintained at 1.00 when one of the variables in the group was altered by dividing the change equally between other variables in the group

Variable (X)	Value	Uncertainty (ΔX)	Percent change in area >5 g POC m^{-2} d^{-1} $-\Delta X$	$+\Delta X$
Farm site and husbandry variables				
Z_m (m)	18.4	5.5	−63.5	58.5
$\bar{U}_{mean}$ (cm s^{-1})	9.20	4.11	−23.6	51.5
T_{max} (°C)	12.83	1.50	−23.6	22.9
TGC ($g^{1/3}°C^{-1}$ d^{-1})	2.368×10^{-3}	0.2×10^{-3}	−14.3	20.3
SD (kg m^{-3})	17.2	2.4	−5.0	18.9
T_{min} (°C)	0.75	0.1	−0.3	2.0
JD_{Tmin}	70	5	11.3	−0.3
f_{mort}	0.15	0.05	8.3	−0.3
Mass-balance coefficients				
DM_{fish}	0.36	0.02	−0.3	9.3
f_{Cfish}	0.54	0.02	−0.3	4.7
f_{Cinput}	0.38	0.03	19.3	−1.7
$f_{Crespired}$	0.40	0.03	−0.3	−0.3
f_{Cfeces}	0.19	0.03	−13.6	19.6
$f_{Cwastefeed}$	0.03	0.03	2.0	−0.3
Particulate waste mass fractions and settling velocities				
f_{feces1}	0.66	0.05	−17.3	0.3
f_{feces2}	0.25	0.05	9	−19.6
f_{feces3}	0.09	0.05	−7.0	0.3
w_{pt1}	10	2.0	0	0
w_{pt2}	7.5	2.5	40.9	−5.7
w_{pt3}	3	2	−28.9	−19.6
w_{pt4}	0.5	0.25	−0.3	4.3
Net sedimentation				
f_{decomp}	0.1	0.1	9.5	−14.3
f_{cons}	0.5	0.25	0	0
$B_{sub1\ mean}$ (cm s^{-1})	9.2	4.11	−19.1	−1.0
$B_{sub2\ mean}$ (cm s^{-1})	9.2	4.11	−19.1	28.6
$B_{sub3\ mean}$ (cm s^{-1})	9.2	4.11	−19.1	47.6

3.4. Factors affecting waste deposition areas

Results of changes in current speed, under-pen depth and the number of fecal fractions with different settling velocities applied at Farm A are consistent with results using the analytical Gaussian dispersion model in Stucchi et al. (2005) (Fig. 4). The actual magnitude of model output values for maximum waste discharge and areas receiving different levels of waste deposition depend on the number of fish, net-pen dimensions, depth and current speed. Maximum sedimentation is greater for a given current speed when under-cage depth is shallow (8.4 m) than when it is deeper (30 m) since waste is dispersed over a larger area (Fig. 4A,C). Areas for a given deposition rate increase to maxima with increasing current and if water depth is sufficiently deep the areas for the lowest flux rate disappear. Although waste is deposited into the larger area due to high current speeds, the flux rate falls below the threshold for the lowest contour level (>1 g POC m^{-2} d^{-1}). As Stucchi et al. (2005) observed, the patterns for changes in current speed are similar to those when depth is varied. Deeper depths, like high currents, increased the area of waste dispersion to maxima, above which areas for lower rates of flux decrease and eventually disappear.

The rationale for selecting mass fractions of feces with different settling rates is discussed in Supplement 1. Results for a single fecal type with a settling rate of 3.0 cm s^{-1} are based on mass fractions used by Stucchi et al. (2005) to represent the mean and standard deviation (3.2 ± 1.1 cm s^{-1}) applied in DEPOMOD (Cromey et al. 2002a) (Fig. 4A). Since Bannister et al. (2016) showed in laboratory experiments that most (58–78%) salmon feces settle at >5 cm s^{-1} with a smaller slow settling fraction <1 cm s^{-1}, we used 3 fractions (0.66, 0.25, 0.09) to span this range (w = 7.5, 3.0, 0.5 cm s^{-1}, respectively) (Table 1). It is possible that under *in situ* conditions proportions of feces in the finer fractions could be higher as a result of shear effects on larger fecal pellets. When the broader distribution of fecal types is used, the areas of waste dispersion change. Maximum sedimentation immediately under a net-pen is lower than calculated using a single fecal fraction for a shallow depth (Fig. 4B vs. A) with a further decrease with increasing currents at a deeper depth (Fig. 4D vs. C). Areas for different flux levels continue to increase as current increases but differ for different levels of flux. The inclusion of fecal fractions with lower settling rates increases

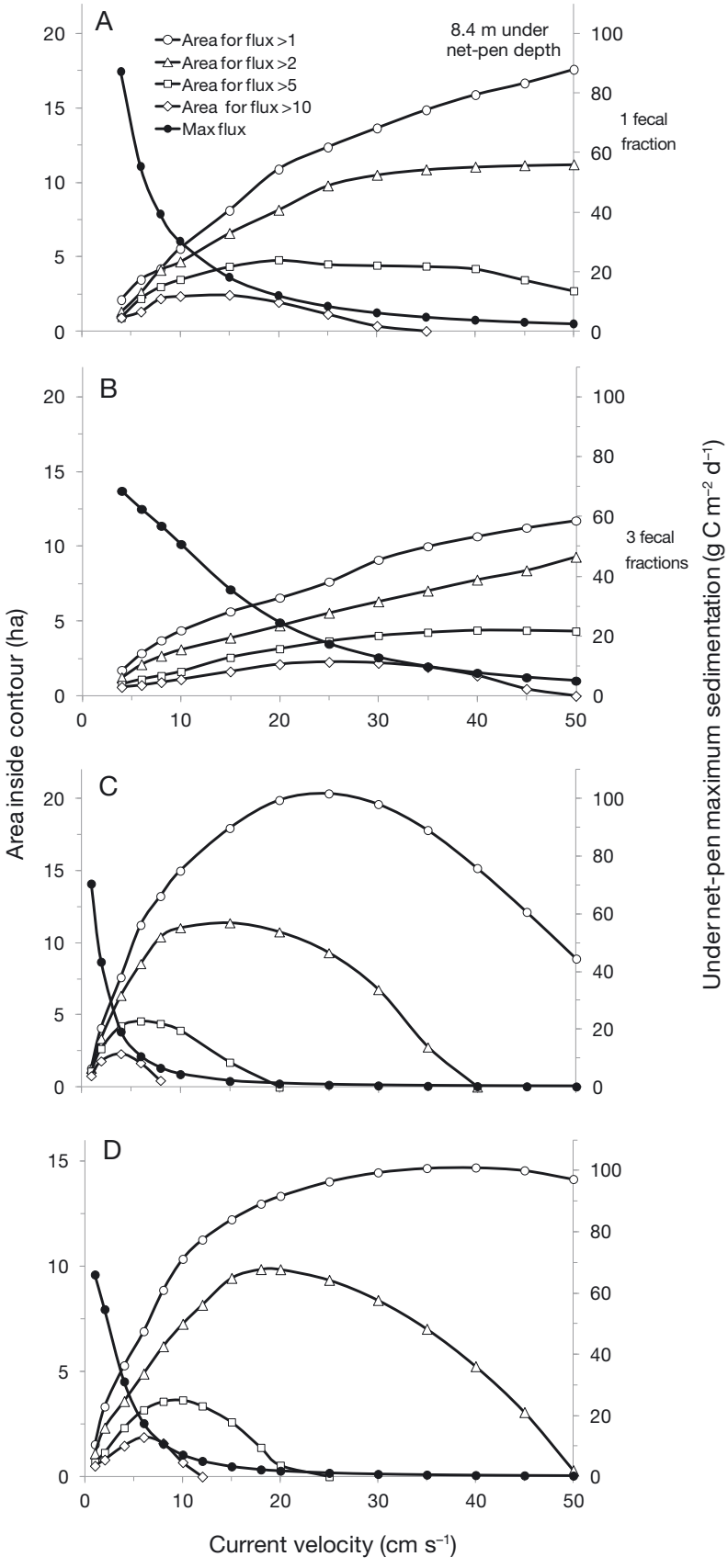

Fig. 4. Model output for maximum total POC waste sedimentation for Farm A in Bliss Harbour integrated for the area under the net-pen array and various sedimentation rate contour areas with changes in current speed, under net-pen depth and number of fecal size fractions. Allowable production limit: 330 000, mortality: 15% with no corrections for resuspension, decomposition or waste feed consumption in all comparisons. (A) 1 fecal size fraction, settling speed (w) 3.2 cm s^{-1} and (B) 3 fecal size fractions (0.66, 0.25 and 0.09; w = 7.5, 3.0 and 0.5 cm s^{-1}) with 8.4 m under-pen depth; (C,D) the same 1 and 3 fecal size fractions but with 30 m under-pen water depth. Model area is 100 ha with a 10 m grid resolution

the maximum size of waste depositional footprint as current speed increases.

3.5. Factors affecting spatial patterns of waste deposition

Maximum total and net particulate waste sedimentation for contour intervals <3 and >10 g POC m^{-2} d^{-1} for the multi-pen matrix in Farm A using one fecal size fraction are shown as contour plots in Fig. 5. Calculated areas for maximum total and net waste sedimentation >0.3 and >5 g POC m^{-2} d^{-1} and integrated values immediately under net-pens dimensions for this and following model scenarios are listed in Table 4. Deposition within the modelled area (600 × 600 m, 36 ha, 6 × 6 m cell resolution) represents 100% of the waste released using the mean depth of 18.4 m (8.4 m under-cage depth) at Farm A. Depth-average current statistics from Table 2 were applied for June–August (Fig. 5A,B), September–November (Fig. 5C,D) and September–November (Fig. 5E,F) when near-surface currents were decreased (×0.5) and mid- and near-bottom current increased (×2) to account for net-pen effects (Wu et al. 2014).

Contours for all intervals of POC flux around individual net-pens within the array have similar circular and slightly skewed shapes, reflecting small differ-

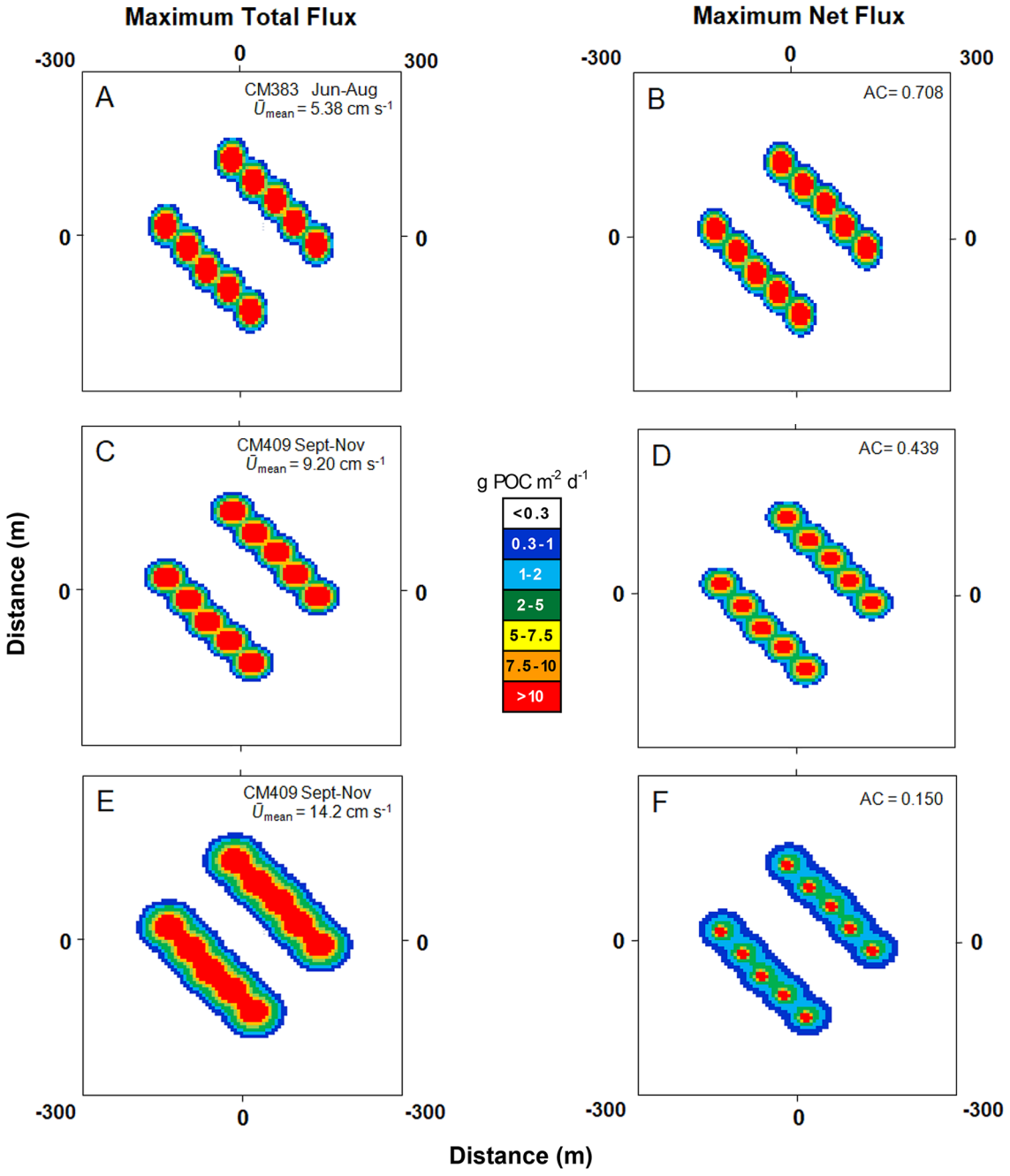

Fig. 5. Model output for contour areas for 2 levels of POC sedimentation (<0.3 and >5 g POC m^{-2} d^{-1}, shown in Table 4) for total and net waste flux and maximum deposition integrated over the area under net-pens based on one fecal size fraction (settling speed w = 3.2 cm s^{-1}), mean depth of 18.4 m (8.4 m under cages) and depth-average currents ($\bar{U}_{mean}$) for (A,B) June–August (CM383), (C,D) September–November (CM409) and (E,F) September–November (CM409) with near-surface currents decreased (×0.5) and mid- and near-bottom current increased (×2) to account for net-pen side wall drag effects (Wu et al. 2014) (Table 2). Variables for stocking number mortality during the grow-out period, waste feed and losses due to resuspension, decomposition and consumption of waste feed by wild fish and invertebrates in Table 1. Model area is 36 ha with a 6 m grid resolution. Assimilation coefficient (AC) is the ratio of net to total waste flux. The ratio in (B) indicates that 70.8% of deposited waste remains in the model area after losses due to resuspension, decomposition and consumption

ences in σ_{EW} and σ_{NS} (Table 2). Contours for >5 g POC m^{-2} d^{-1}, separated under individual cages at lower currents in June–August (Fig. 5A,B), overlap when higher currents associated with under-cage accelerated currents are applied for the September–November period (Fig. 5E,F). The areas of max-

Table 4. Contour areas shown in Figs. 5–9 for net-pens containing Atlantic salmon at Farm A for 2 levels of total and net waste sedimentation and integrated flux under single net-pens for maximum waste production during the grow-out period. Sedimentation threshold values selected to represent background sedimentation (<0.3 g POC m^{-2} d^{-1}) and enhanced flux associated with benthic enrichment (>5 g POC m^{-2} d^{-1}) are discussed in Section 2.3 and Supplement 1

Figure	Total flux area (ha)		Net flux area (ha)		Under net-pens	
	<0.3	>5	<0.3	>5	Total flux	Net flux
	g POC m^{-2} d^{-1}		g POC m^{-2} d^{-1}		g POC m^{-2} d^{-1}	
5 A,B[a]	4.18	2.25	3.93	1.92	45.0	30.9
5 C,D	4.40	2.43	3.87	1.57	41.0	17.7
5 E,F	7.01	3.51	4.77	0.55	59.4	9.14
6 A,B	7.00	1.08	3.75	0.89	56.7	46.7
6 C,D	7.43	1.08	3.25	0.76	52.5	33.5
6 E,F	7.48	1.64	2.88	0.75	44.2	11.9
7 A,B	6.43	0.83	1.78	0.40	63.2	33.7
7 C,D	8.42	2.04	5.02	1.33	38.9	21.7
7 E,F	12.10	3.25	7.07	2.22	20.7	11.4
8 A,B	5.10	1.33	2.88	0.75	21.7	11.9
8 C,D	5.10	1.66	2.89	0.97	28.4	20.8
8 E,F	5.10	1.70	3.10	1.12	29.7	29.9
9 A,B	7.05	1.25	5.52	1.65	53.5	24.9
9 C,D	7.05	1.25	8.79	1.55	53.5	24.9

[a]A summary of model output data for this scenario is shown in Supplement 2

imum total flux (>0.3 and >5 g POC m^{-2} d^{-1}) increase only slightly between the June–August and September–November mooring periods (Fig. 5A,C) but higher depth-average currents due to under-cage acceleration increases the size of both areas in September–November (Fig. 5E). Integrated values for maximum total sedimentation (41–45 g POC m^{-2} d^{-1}) at lower currents decrease to 25 g POC m^{-2} d^{-1} when higher currents are considered (Fig. 5A,C,E).

Net maximum fluxes respond differently to changes in current speed. Contour areas >0.3 and >5 g POC m^{-2} d^{-1} are only slightly reduced by the increase in depth-average currents between June–August and September–November (Fig. 5B,D), but much larger changes occur when higher under-cage velocities are applied (Fig. 5F). The total footprint area (>0.3 POC m^{-2} d^{-1}) increases, but the area >5 g POC m^{-2} d^{-1} is drastically reduced. The differences reflect the effects of resuspension on net waste flux. With lower currents during the first mooring period, the AC indicates that 70.8% of maximum total flux would remain deposited after losses due to resuspension, decomposition and consumption (Fig. 5B). The value decreases to 43.9% as more deposited material is removed with higher currents in September–November (Fig. 5D). A further increase in currents due to under-cage acceleration results in net sedimentation being only 14.7% of total flux (Fig. 5F). The magnitude of the loss of deposited material is evident by changes in both the >5 g POC m^{-2} d^{-1} contour area and mean flux under net-pens, which are both reduced by an order of magnitude.

The predicted contour areas for maximum total flux >5 g POC m^{-2} d^{-1} without consideration of net-pen effects for the 2 current meter mooring periods are 2.25 and 2.43 ha (Fig. 5A,C). A lower value (1.27 ha) was calculated for this depositional contour area when DEPOMOD was applied at Farm A using feeding rates from 2007 and currents measured between June and August 2009 (CM-D1 in Chang et al. 2014a). The discrepancy is not related to differences in current velocities since depth-averaged currents from CM-D1 ($\bar{U}_{median}$ = 4.97 cm s^{-1}) are similar to observations with CM383 ($\bar{U}_{median}$ = 5.15 cm s^{-1}) (Table 2). The comparison of feeding rates, however, shows that the industry-reported 1 mo average feeding rate in the final year of production in July 2007, used in the DEPOMOD model, was approximately 50% lower than the maximum values we use in our worst-case calculations for September–November in the second year of production (Fig. 2B). When feeding rates in our model were reduced by 50%, the >5 g POC m^{-2} d^{-1} contour area was 1.61 ha. The estimated area >5 g POC m^{-2} d^{-1} in DEPOMOD calculations with resuspension using a 9.5 cm s^{-1} current threshold for a single fecal size class was 1.05 ha (Chang et al. 2014a). The smaller area may reflect the fact that DEPOMOD only allows resuspended particles to resettle when resuspension is turned on if particles remain within the model domain. The recalculated value for total net sedimentation for the >5 g POC m^{-2} d^{-1} area in our study using a single fecal type (w = 3.0 cm s^{-1}) and the lower feeding rate comparable to that used in DEPOMOD is 1.26 ha.

The result of erosion and dispersal of deposited waste particles as currents increase and shear velocities exceed the critical erosion threshold (τ_{crit}) (Law et al. 2016) is shown by changes in AC ratios. During the period of lower currents (June–August) with one fecal fraction the ratio is 0.708 (Fig. 5B), indicating that 29% of deposited waste particles are removed from the modelled area by resuspension, decomposi-

tion and consumption. With increased currents in September–November (Fig. 5D) (AC = 0.439), 56% of the waste released remains deposited. With higher near-bottom currents due to cage effects (Fig. 5F) (AC = 0.147), approximately 85% of deposited material is lost from the modelled area. The net/total ratio (AC) indicates that with low currents most of the waste already deposited remains on the bottom under or close to net-pens, but higher currents will remove a large fraction of sedimented material. Keeley et al. (2019) also calculated that a large fraction (60–70%) of waste output from a salmon farm at a shallow dispersive location on the west coast of Norway was assimilated in the water column, consumed by fish and invertebrates or exported and dispersed from the farm site. Waste accumulation has been observed under cages at Farm B and other farm sites in SWNB. However, comparisons of rates of waste discharge and sediment–water fluxes of O_2, CO_2 and dissolved nitrogen showed that while some waste is buried, a large fraction is lost by resuspension, decomposition and solubilization (Strain & Hargrave 2005).

Contours for maximum total and net sedimentation with 3 current velocities and one fecal fraction (Fig. 5) are replicated using 3 fecal fractions and their respective settling velocities (Table 1) in Fig. 6A–F. The circular contour areas >5 g POC m^{-2} d^{-1} resulting from applying 3 fecal fractions in our model are similar in shape to those using one fecal fraction, but the areas are reduced. The change is consistent with the high combined mass fraction of large (0.66) and small (0.25) feces with relatively high settling velocities (7.5 and 3.0 cm s^{-1}, respectively). The larger and more rapidly settling fecal fractions reach the bottom quickly and are deposited in a smaller area. Contour areas >0.3 g POC m^{-2} d^{-1} show an opposite effect with an increase in contour area resulting from the inclusion of flocculated fine fecal matter with a low (0.5 cm s^{-1}) settling velocity.

Effects of current speed on AC ratios for 1 and 3 fecal fractions are generally similar, showing a decrease due to higher losses by resuspension as current velocities increase (Fig. 6B,D,F), but the ratios are slightly higher using 3 fecal fractions. The range of current velocities and total maximum waste produced by the farm are the same for model outputs in Figs. 5 & 6, so differences in the AC ratios reflect effects of resuspension that affect net but not total sedimentation. Use of 3 different mass fractions for fecal types with different settling rates and τ_{crit} thresholds decreases losses due to resuspension. The decrease is evident in differences in under-cage maximum integrated fluxes. With one fecal fraction, values decrease from 30.9 at low currents to 3.8 g POC m^{-2} d^{-1} at higher velocities due to near-bottom cage effects (Fig. 5B,F). The corresponding change for 3 fecal fractions is a decrease from 45.7–11.2 g POC m^{-2} d^{-1} (Fig. 6B,F). Different τ_{crit} thresholds applied for large (w_{pt2}) and small (w_{pt3}) sized fecal pellets (Table 1) result in less resuspension than calculated using the single value in DEPOMOD for one fecal waste type (9.5 cm s^{-1}) As a result, for a given current, net deposition increases when 3 fecal fractions are considered.

The generally circular shapes of depositional contours within the farm cage array immediately under net-pens are maintained but increase in size with increasing depth (Fig. 7A,C,E). As depth increases, settling particles with a specified settling rate (w) require a longer time to reach the bottom, and as a result, are transported over greater horizontal distances (Eq. S3 in Supplement 1). Although the model is not intended to show fluctuations in waste sedimentation over a tidal cycle, hence the use of a mean value for lowest normal tide (Z_m) as input data (Table 1), depths associated with minimum, mean and maximum tides for the farm in Bliss Harbour (Chang et al. 2014a) can be used to illustrate changes in the size of the waste depositional footprint during a tidal cycle (Fig. 7). Both maximum total and net fluxes for >0.30 and >5 g POC m^{-2} d^{-1} contour areas increase from minima with 2.9 m under-cage depth (Fig. 7A,B) to maxima for the depth at high tide (13.9 m under-cage depth) (Fig. 7E,F) using depth average mean currents to represent net-pen effects ($\bar{U}_{mean}$ = 8.21 cm s^{-1}) (Table 2). The proportion of maximum total sedimentation resuspended (AC = 0.497) remains the same for all depths (Fig. 7B,D,F) since the same erosion velocity thresholds are applied irrespective of depth. Maximum integrated waste flux under net-pens decreases as water depth increases due to greater horizontal dispersion of settling particles. Increased horizontal transport of waste is shown by increasing areas of both the >0.3 and >5 g POC m^{-2} d^{-1} depositional contours as depth increases.

3.6. Substrate effects on net waste flux

Application of different erosion thresholds for waste feed and 3 fecal size classes deposited on mud, sand and gravel substrates (Table 1) at low current velocities with cage effects on near-bottom currents

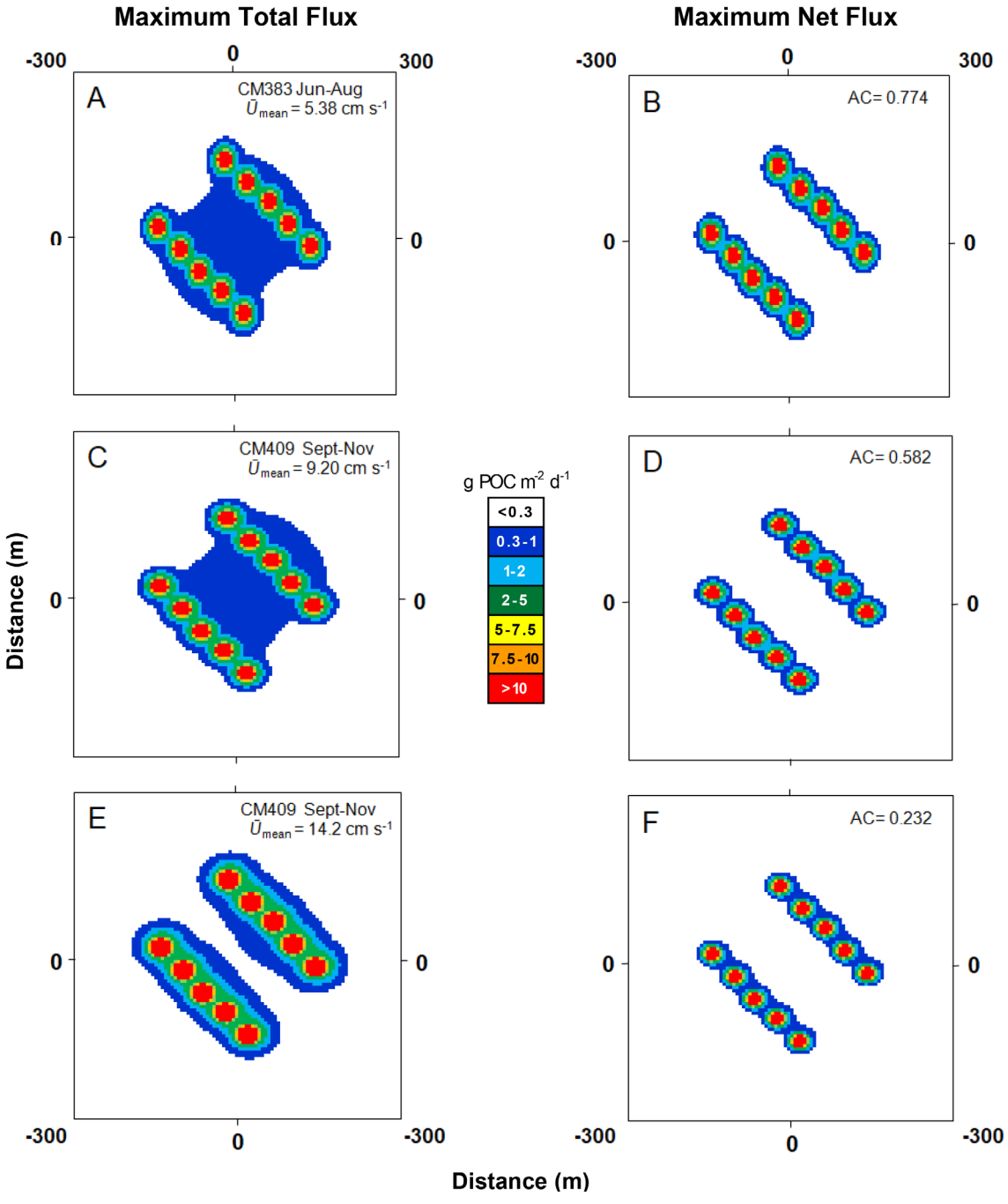

Fig. 6. Model output for the same 2 enrichment contour intervals and maximum under-cage POC flux for total and net waste sedimentation for the model area and grid resolution as applied in Fig. 5 but using statistics for 3 different current speeds and 3 fecal size classes with mass fractions and settling velocities described in Fig. 4B

between June and August ($\bar{U}_{mean}$ = 8.21 cm s^{-1}) has no effect on maximum total flux contour areas >0.3 g POC m^{-2} d^{-1} (Fig. 8A,C,E). However, the area for >5 g POC m^{-2} d^{-1} increases (24%) across the 3 substrate types. At higher currents in September–November $\bar{U}_{mean}$ = 14.2 cm s^{-1}) (Fig. 8B,D,F), both areas increase much less for the >0.3 POC m^{-2} d^{-1} area (8%) than for >5g POC m^{-2} d^{-1} (36%). The differences reflect the interactions between changes in current speed and the proportion of time near-bottom velocities exceed resuspension thresholds for different substrate types. Waste feed and large and small fecal pellets predominate deposited waste immediately under net-pens, resulting in the largest

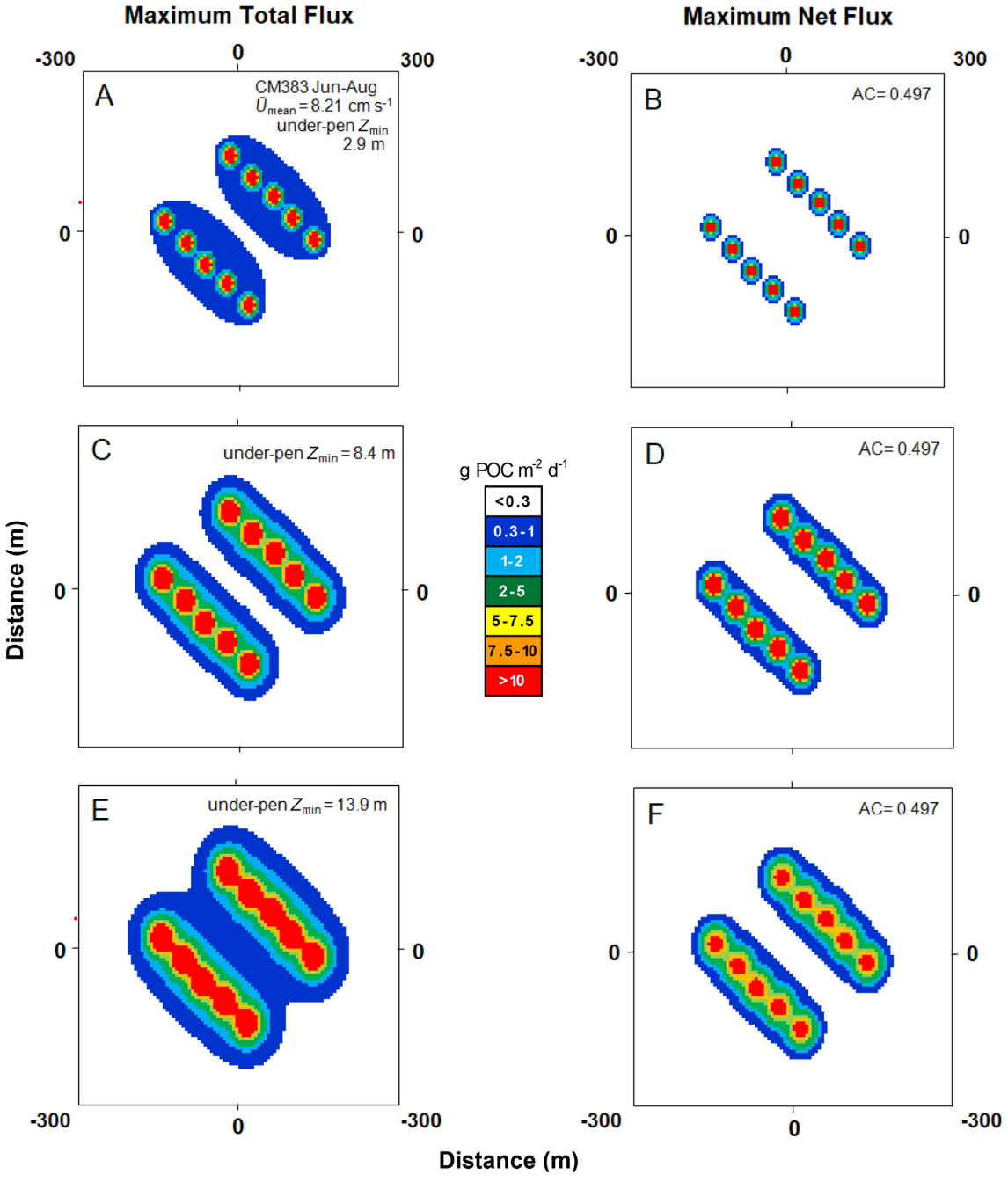

Fig. 7. Model output for 2 enrichment contour intervals and maximum total and net POC flux under net-pens as in Fig. 6 for 3 fecal size classes but with current statistics from CM383 modified for net-pen side-wall drag effects (Table 2) and 3 under-pen depths. Z_{min} is Z_m corrected for NP_z (Table 1). Addition of NP_z (10 m) represents minimum, mean and maximum under-cage depths for a normal tide in Bliss Harbour (Chang et al. 2014a)

changes in footprint size in the high flux contour area. Flocculated fecal material with a slower settling rate is transported away from below-cage areas of high flux. Differences in net flux between substrate categories also reflect higher erosion velocities required to resuspend waste feed and feces deposited on sand (22.5 cm s^{-1}) and gravel (35 cm s^{-1}) as opposed to mud (15 cm s^{-1}) (Table 1). Higher current speeds remove proportionately more deposited waste from mud substrates than gravel due to the higher erosional velocity required for resuspension from the latter substrate.

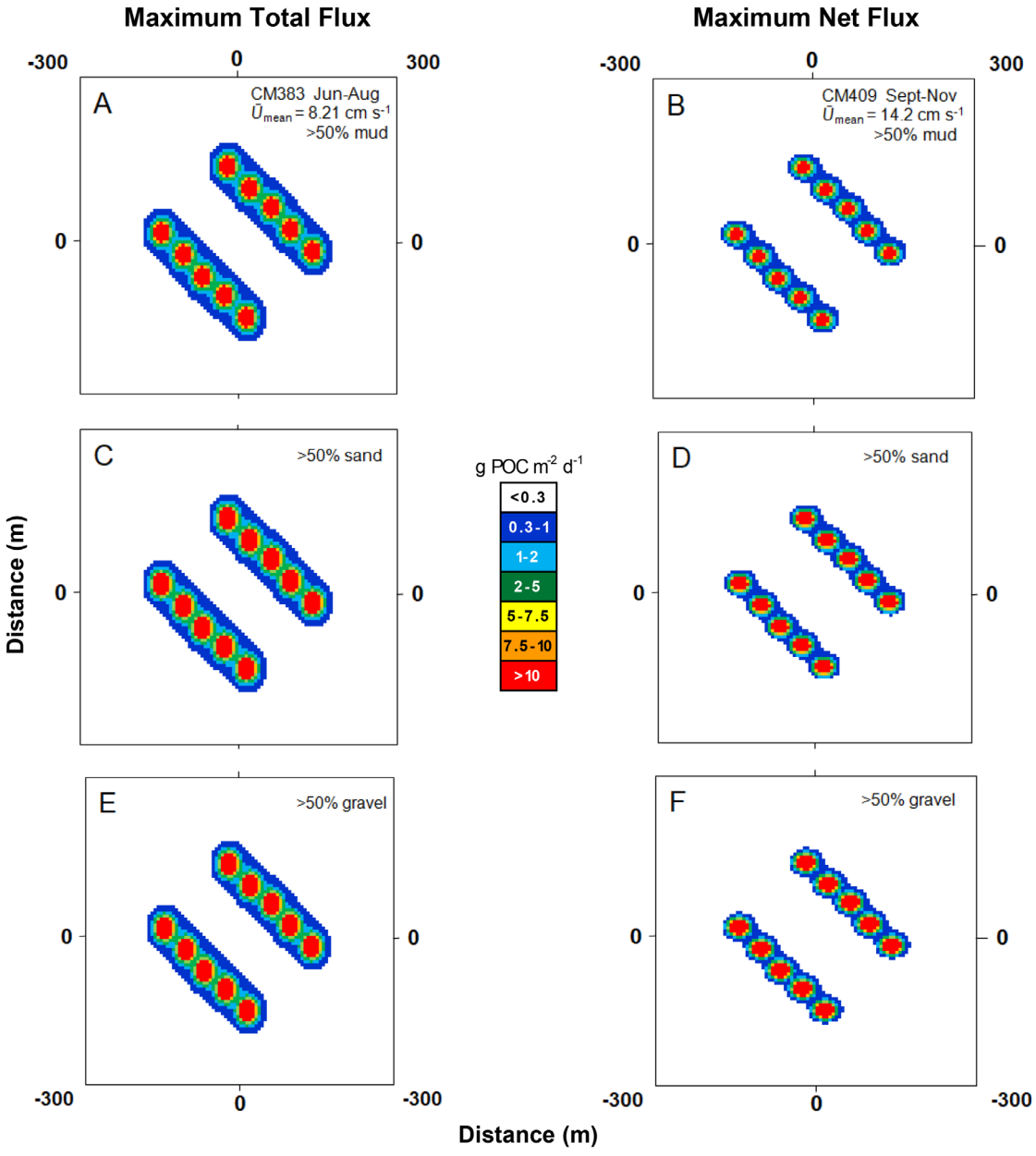

Fig. 8. Model output for 2 enrichment contour intervals and maximum net POC flux under net-pens applying 3 fecal size classes and current statistics from (A,C,E) CM383 and (B,D,F) CM409 modified for net-pen side-wall drag effects (Table 2) for 3 bottom substrate types (A,B) >50% mud, (C,D) >50% sand and (E,F) >50% gravel. Model area is 36 ha with a 6 m grid resolution

3.7. Net-pen array orientation

The orientation of the long axis of the net-pen array relative to the predominant current affects the size and shape of depositional footprints depending on the relative magnitude of σ_{EW} and σ_{NS}. As discussed above, the similarity in these values at Farm A (Table 1) results in circular depositional footprints with highest waste flux under and close to net-pens. In this case, with $\bar{U}_{mean}$ set to 0 (no residual current), rotation of the array long axis to be parallel or perpendicular to the major current has no effect on individual cage depositional contour shapes or sizes relative to the array center position (Fig. 9A,C). The area where more slowly settling particles are deposited between rows of cages, however, is rotated 90°.

The effect of array rotation on depositional areas is very different if σ_{EW} and σ_{NS} are not the same (Fig. 9B,D). If the predominant current is east–west

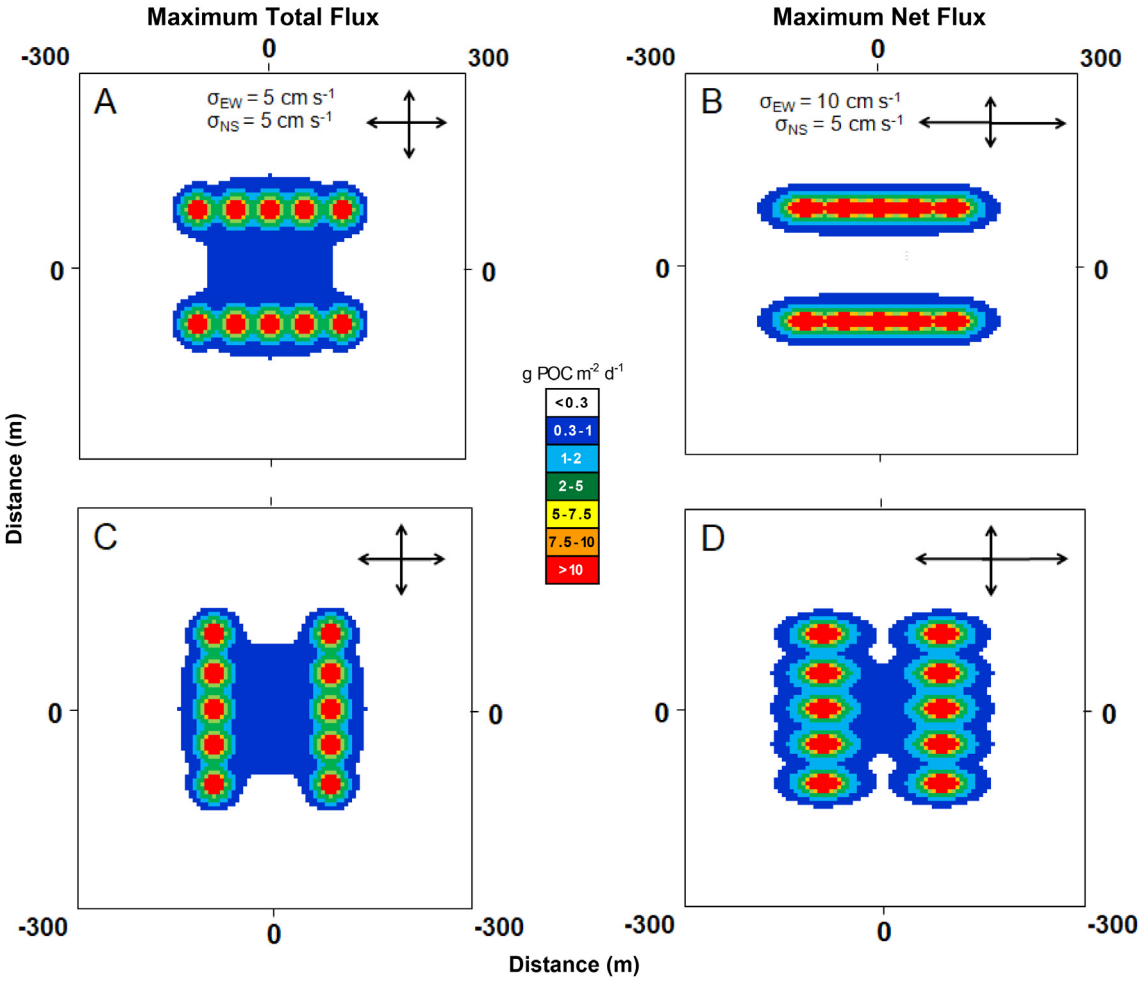

Fig. 9. Model output for depositional areas and maximum total and net POC flux with changes in net-pen array orientation to the predominant current direction. Model variables as in Fig. 7C (under net-pen depth: 8.4 m; 3 fecal size classes) but mean currents (μ_{EW} and μ_{NS}) = 0. (A,B) Long axis of the net-pen array parallel to the predominant EW current, (C,D) perpendicular orientation. (A,C) Equal standard deviations for directional currents (σ_{EW} and σ_{NS}), (B,D) σ_{EW} increased ×2. Arrows illustrate the relative magnitude of current standard deviations

(σ_{EW} 2× > σ_{NS}), as in this example, the depositional footprints for all levels of waste flux are elongated in the direction of the major current. The contour areas immediately under and adjacent to cages are elongated in the direction of the predominant current. As mentioned above, with no residual current there is no offset for maximum flux at the center position of each cage. A residual current would move all depositional contour areas from the center position in the direction of the residual current with a magnitude in the shift proportional to the current, as shown in Cubillo et al. (2016). Similar differences in footprint shape and area with a change in array orientation from parallel to perpendicular to the major current were observed when the Gaussian dispersion model was applied in the Broughton Archipelago, where σ_{EW} was 4 times greater than σ_{NS} (Stucchi et al. 2005).

3.8. Comparison of predicted maximum total waste flux and sediment trap observations

No sediment trap observations were made between 2005 and 2007 at Farm A for comparison with predicted outputs from our model or results from DEPOMOD described in Chang et al. (2014a). However, traps suspended at Farm B (Fig. 1) provided data to compare with predicted values for maximum total waste sedimentation without resuspension. Farm configuration (number and sizes of cages, array dimensions) and stocking number (APL) were adjusted to apply our model at Farm B at the time of sediment trap deployments (see Section 2.1). APL was increased by 10% (120 000) to account for over-stocking, and a mortality rate of 15% over the grow-out period assumed for Farm A (Table 1) was applied. Cur-

rents for the summer period of lower currents (June–August) (CM383) adjusted for lower surface layer and increased near-bottom velocities due to cage effects (Table 2) corresponded to the period when sediment traps were deployed (19–24 August 1990).

The range of sedimentation rates measured at 2 locations within the cage array, 2 at the edge and at reference locations 25 and 50 m away from the array (15–0.3 g POC m^{-2} d^{-1}) is consistent with steep gradients in maximum total sedimentation contour areas predicted around the net-pen array for both 1 and 3 fecal waste types (Table 5). Predicted fluxes in cells in the depositional matrix corresponding to trap mooring locations with 1 and 3 fecal fractions span a similar order of magnitude range from under and up to 50 m away from the net-pen array. Predicted and observed fluxes are significantly correlated ($p < 0.05$) for both 1 and 3 waste types but the slope of the regression between observed (x) and predicted (y) values was closer to 1 for 3 ($y = 1.350 + 1.110x$, $r^2 = 0.902$) as opposed to 1 fecal fraction ($y = 3.001 + 2.203x$, $r^2 = 0.908$).

Table 5. Observed sedimentation rates (n = 4) (mean and SE in parentheses) at 6 locations at Farm B (19–24 August 1990) in Bliss Harbour (Fig. 1) from Hargrave (1994) compared to predicted maximum total POC sedimentation in model cells corresponding to trap mooring positions. Traps were suspended at 13.5 m, the value used for mean lowest normal tide depth (Z_m). Current statistics account for net-pen drag and near-bottom current acceleration effects (depth-average $\bar{U}_{mean}$ = 8.21 cm s^{-1}) (Table 2) applied for model scenarios with 1 and 3 fecal size fractions (w) (Table 1). Grid resolution is 6 × 6 m in a 36 ha model area. POC flux +50 m from the net-pen array, considered to be background sedimentation, is included in predicted values. Fecal size fractions are described in Table 1

Trap location	Sedimentation rate (g POC m^{-2} d^{-1})		
	Observed	Predicted	
		w_{pt2}	$w_{pt2}+w_{pt3}+w_{pt4}$
1 (array interior)	15.0 (4.6)	33.04	14.56
2 (array interior)	7.8 (3.6)	25.67	12.50
3 (array edge)	1.4 (0.4)	8.60	3.12
4 (array edge)	1.2 (0.2)	8.48	3.08
5 (+25 m from array)	0.8 (0.2)	0.30	0.56
6 (+50 m from array)	0.3 (0.1)	0.30	0.32

4. CONCLUSIONS

Previously described models for temperature-dependent fish growth, mass-balance estimates of food intake, respiration and particulate waste production are combined with a statistical waste dispersion–deposition model in an MS Excel® spreadsheet format to predict particulate waste sedimentation at 2 Atlantic salmon farms in SWNB, Bay of Fundy. Unlike DEPOMOD, the spreadsheet format allows all site physical and farm husbandry variables to be varied to consider integrated effects of changes in the degree and spatial patterns of particulate waste deposition due to salmon aquaculture. Model results are generally consistent with DEPOMOD model output for Farm A. Sediment trap results from Farm B are similar to model-predicted values for similar positions under, adjacent to and up to 50 m from the net-pen array when stocking number, cage dimensions and spacing were adjusted for conditions at the time of sediment trap observations.

Stocking number, water depth, variations in mean and standard deviations in current speed, waste mass fractions and particle settling velocities are the major factors determining rates and spatial patterns of waste feed and feces sedimentation. Boundaries for specified depositional contours show highest sedimentation under and adjacent to net-pens, reflecting rapidly settling unconsumed feed and large fecal pellets. Smaller fecal pellets and disaggregated fecal matter with lower settling velocities are deposited up to 50 m from the net-pen array.

The combined models for fish growth, waste production, dispersion and deposition of particulate waste from salmon aquaculture can be used by industry managers, government regulators and non-governmental organizations to directly evaluate new or established salmon farms to assess site suitability and manage negative effects of increased organic waste deposition under and near net-pens. Unlike DEPOMOD, where information is required for individual net-pens, the spreadsheet model uses general temperature–growth and mass-balance calculations to calculate feed input requirements. The model provides regulators with an assessment of feed input to support calculated growth independent of industry-reported values. The uniform spatial patterns of waste deposition assumed that salmon biomass is the same in all cages, but the number of net-pens can be altered to account for changes in farm size if required for management purposes.

Application of the spreadsheet model requires new information to categorize mass fractions of feces of different sizes and settling rates. It is known that different settling velocities of waste feed and fecal material released by salmon directly affect the size of the waste depositional footprint (Bannister et al. 2016), but few previous studies have provided the

necessary information to determine mass fractions of different-sized waste particles. Complexities for parameterizing resuspension remain. For example, while the erosion thresholds we have used are practical, freshly deposited material on the surface has a very low erosion threshold compared to that incorporated into sediment interstices. The latter is more dependent on the movement of the background sediment, as in the present model. New field observations are required to assess mass fraction distributions of different sizes of waste particles and resuspension thresholds for freshly produced fecal material under *in situ* conditions to more accurately determine the size and shape of depositional footprints.

Acknowledgements. We thank S. Robinson for providing seasonal water temperature data from Passamaquoddy Bay monitoring stations used for growth calculations. We are grateful to F. Page, R. Losier and B. Chang for access to ADCP current meter data from 2 moorings at Farm A from their study in 2009. B. Chang confirmed Farm A dimensions and stocking levels in 2009 at the time of current meter deployments and suggested mortality rates over the grow-out period representative of the salmon aquaculture industry in SWNB. D. Wildish and B. Chang provided comments on an early draft of the manuscript and H. Koepke verified details of model calculations.

LITERATURE CITED

Adams TP, Black K, Carpenter T, Hughes AD, Reinardy HC, Weekes RJ (2020) Parameterizing resuspension in aquaculture waste deposition modelling. Aquacult Environ Interact 12:401–415

Aunsmo A, Krontveit R, Valle PS, Bohlin J (2014) Field validation of growth models used in Atlantic salmon farming. Aquaculture 428–429:249–257

Bannister RJ, Johnsen IA, Hansen PK, Kutti T, Asplin L (2016) Near- and far-field dispersal modelling of organic waste from Atlantic salmon aquac ulture in fjord systems. J Mar Sci 73:2408–2419

Black KD, Carpenter T, Berkeley A, Black K, Amos C (2016) Refining sea-bed process models for aquaculture. SAM/004/12. https://www.sams.ac.uk/t4-media/sams/pdf/publications/REFINING-SEA-BED-PROCESS-MODELS-FOR-AQUACULTURE-Final-Report-for-web.pdf

Brigolin D, Pastres R, Tomassetti P, Porrello S (2010) Modelling the biomass yield and the impact of seabream mariculture in the Adriatic and Tyrrhenian Sea (Italy). Aquacult Int 18:149–163

Broch OJ, Daae RL, Ellingsen IH, Nepstad R, Bendiksen EÅ, Reed JL, Senneset G (2017) Spatiotemporal dispersal and deposition of fish farm wastes: a model study from central Norway. Front Mar Sci 4:199

Callier MD, Byron CJ, Bengtson DA, Cranford PJ and others (2018) Attraction and repulsion of mobile wild organisms to finfish and shellfish aquaculture: a review. Rev Aquacult 10:924–949

Carvajalino-Fernández MA, Sævik PN, Johnsen IA, Albretsen J, Keeley NB (2020) Simulating particle organic matter dispersal beneath Atlantic salmon fish farms using different resuspension approaches. Mar Pollut Bull 161: 111685

Chamberlain J, Stucchi D (2007) Simulating the effects of parameter uncertainty on waste model predictions of marine finfish aquaculture. Aquaculture 272: 296–311

Chang BD, Page FH, Losier RJ, McCurdy EP (2014a) Organic enrichment at salmon farms in the Bay of Fundy, Canada: DEPOMOD predictions versus observed sediment sulphide concentrations. Aquacult Environ Interact 5: 185–208

Chang BD, Coombs KA, Page FH (2014b) The development of the salmon aquaculture industry in southwestern New Brunswick, Bay of Fundy, including steps toward integrated coastal zone management. Aquac Econ Manag 18:1–27

Cromey CJ, Black KD (2005) Modelling the impacts of finfish aquaculture. In: Hargrave BT (ed) Environmental effects of marine finfish aquaculture. Handbook of environmental chemistry, Vol 5, Part M. Springer-Verlag, Berlin, p 129–156

Cromey CJ, Nickell TD, Black KD (2002a) DEPOMOD — modelling the deposition and biological effects of waste solids from marine cage farms. Aquaculture 214:211–239

Cromey CJ, Nickell TD, Black KD, Provost PG, Griffiths R (2002b) Validation of a fish farm waste resuspension model by use of a particulate tracer discharged from a point source in a coastal environment. Estuaries 25: 916–929

Cromey CJ, Thetmeyer H, Lampadariou N, Black KD, Kogeler J, Karakassis I (2012) MERAMOD: predicting the deposition and benthic impact of aquaculture in the eastern Mediterranean Sea. Aquacult Environ Interact 2: 157–176

Cubillo AM, Ferreira JG, Robinson SMC, Pearce CM (2016) Role of deposit feeders in integrated multi-trophic aquaculture: a model analysis. Aquaculture 453:54–66

Føre M, Alver A, Alfredsen JA, Marafioti G and others (2016) Modelling growth performance and feeding behavior of Atlantic salmon (*Salmo salar* L.) in commercial-size aquaculture net-pens: model details and validation through full-scale experiments. Aquaculture 464:268–278

Hargrave BT (1994) A benthic enrichment index. Can Tech Rep Fish Aquat Sci 1949:79–91

Hargrave BT (2010) Empirical relationships describing benthic impacts of salmon aquaculture. Aquacult Environ Interact 1:33–46

Hargrave BT, Duplesia DE, Pfeiffer E, Wildish DJ (1993) Seasonal changes in benthic fluxes of dissolved oxygen and ammonium associated with marine cultured Atlantic salmon. Mar Ecol Prog Ser 96:249–257

Holmer M, Wildish D, Hargrave BT (2005) Organic enrichment from marine finfish aquaculture and effects on sediment processes. In: Hargrave BT (ed) Environmental effects of marine finfish aquaculture. Handbook of environmental chemistry, Vol 5, Part M. Springer-Verlag, Berlin, p 181–206

Keeley NB, Cromey CJ, Goodwin EO, Gibbs MT, Macleod CM (2013) Predictive depositional modelling (DEPOMOD) of the interactive effect of current flow and resuspension on ecological impacts beneath salmon farms. Aquacult Environ Interact 3:275–291

Keeley N, Valdemarsen T, Woodcock S, Holmer M, Husa V, Bannister R (2019) Resilience of dynamic coastal benthic ecosystems in response to large-scale finfish farming. Aquacult Environ Interact 11:161–179

Law BA, Hill PS, Maier I, Milligan TG, Page FP (2014) Size, settling velocity and density of small suspended particles at an active salmon aquaculture site. Aquacult Environ Interact 6:29–42

Law BA, Hill PS, Milligan TG, Zions V (2016) Erodibility of aquaculture waste from different bottom substrates. Aquacult Environ Interact 8:575–584

Milligan TG, Law BA (2005) The effect of marine aquaculture on fine sediment dynamics in coastal inlets. In: Hargrave BT (ed) Environmental effects of marine finfish aquaculture. Handbook of environmental chemistry, Vol 5, Part M. Springer-Verlag, Berlin, p 239–251

Peterson RH, Page F, Steeves GD, Wildish DJ, Harmon P, Losier R (2001) A survey of 20 Atlantic salmon farms in the Bay of Fundy: influence of environmental and husbandry variables on performance. Can Tech Rep Fish Aquat Sci 2337:1–117

Rector ME, Weitzman J, Filgueira R, Grant J (2022) Environmental indicators in salmon aquaculture research: a systematic review. Rev Aquacult 14:156–177

Reid GK, Liutkus M, Robinson SMC, Chopin TR and others (2009) A review of the biophysical properties of salmonid faeces: implications for aquaculture waste dispersal models and integrated multi-trophic aquaculture. Aquacult Res 40:257–273

Riera R, Pérez O, Cromey C, Rodriguez M and others (2017) MACAROMOD: a tool to model particulate waste dispersion and benthic impact from offshore sea-cage aquaculture in the Macaronesian region. Ecol Modell 361: 122–134

Robinson SMC (2022) Passamaquoddy Bay monthly conductivity, temperature and depth (CTD) sampling (1989–2018). https://open.canada.ca/data/en/dataset/12184962-7879-4214-aef0-b31162f04a27

SAMS (Scottish Association for Marine Science) (2019) NewDEPOMOD users guide. Scottish Association for Marine Science, Oban

Silvert W, Cromey CJ (2001) Modelling impacts. In: Black KD (ed) Environmental impacts of aquaculture. Sheffield Academic Press, Sheffield, p 154–181

Stewart JE (2005) Environmental management and the use of sentinel species. In: Hargrave BT (ed) Environmental effects of marine finfish aquaculture. Handbook of environmental chemistry, Vol 5, Part M. Springer-Verlag, Berlin, p 409–432

Stigebrandt A, Aure J, Ervik A, Hansen PK (2004) Regulating the local environmental impact of intensive marine fish farming: III. A model for estimation of the holding capacity in the modelling–ongrowing fish farm–monitoring system. Aquaculture 234: 239–261

Strain PM, Hargrave BT (2005) Salmon aquaculture, nutrient fluxes and ecosystem processes in southwestern New Brunswick. In: Hargrave BT (ed) Environmental effects of marine finfish aquaculture. Handbook of environmental chemistry, Vol 5, Part M. Springer-Verlag, Berlin, p 29–58

Stucchi D, Sutherland TA, Levings C, Higgs D (2005) Near-field depositional model for salmon aquaculture waste. In: Hargrave BT (ed) Environmental effects of marine finfish aquaculture. Handbook of environmental chemistry, Vol 5, Part M. Springer-Verlag, Berlin, p 157–180

Sutherland TF, Amos CL, Ridley C, Droppo IG, Petersen SA (2006) The settling behavior and benthic transport of fish feed pellets under steady flows. Estuar Coasts 29: 810–819

Wang X, Olsen LM, Reitan KI, Olsen Y (2012) Discharge of nutrient wastes from salmon farms: environmental effects, and potential for integrated multi-trophic level aquaculture. Aquacult Environ Interact 2:267–283

Wang X, Andersen K, Handå A, Jensen B, Reitan KI, Olsen Y (2013) Chemical composition and release rate of waste discharge from an Atlantic salmon farm with an evaluation of IMTA feasibility. Aquacult Environ Interact 4: 147–162

Wildish DJ, Pohle GW (2005) Benthic macrofaunal changes resulting from finfish mariculture. In: Hargrave BT (ed) Environmental effects of marine finfish aquaculture. Handbook of environmental chemistry, Vol 5, Part M. Springer-Verlag, Berlin, p 275–304

Wildish DJ, Hargrave BT, MacLeod C, Crawford C (2003) Detection of organic enrichment near finfish net-pens by sediment profile imaging at SCUBA-accessible depths. J Exp Mar Biol Ecol 285–286:403–413

Wildish DJ, Hughes-Clarke JE, Pohle GW, Hargrave BT, Mayer LM (2004) Acoustic detection of organic enrichment in sediments at a salmon farm is confirmed by independent groundtruthing methods. Mar Ecol Prog Ser 267:99–105

Wu Y, Chaffey J, Law B, Greenberg DA, Drozdowski A, Page F, Haigh S (2014) A three-dimensional hydrodynamic model for aquaculture: a case study in the Bay of Fundy. Aquacult Environ Interact 5:235–248

Editorial responsibility: Catriona MacLeod, Hobart, Tasmania, Australia
Reviewed by: S. Hadley, T. Adams

Submitted: June 10, 2022
Accepted: October 18, 2022
Proofs received from author(s): November 30, 2022